Mineralogical Magazine, June 2017, Vol. 81(3), pp. 707–722

The crystal chemistry of oxo-mangani-leakeite and mangano-mangani-ungarettiite from the Hoskins mine and their impossible solid-solution: An XRD and FTIR study

Roberta Oberti[1,*], Giancarlo DellaVentura[2], Massimo Boiocchi[3], Alberto Zanetti[1] and Frank C. Hawthorne[4]

[1] CNR-Istituto di Geoscienze e Georisorse, Sede secondaria di Pavia, via Ferrata 1, I-27100 Pavia, Italy
[2] Dipartimento di Scienze, Università di RomaTre, largo S. Murialdo 1, I-00146 Roma, Italy
[3] Centro Grandi Strumenti, Università di Pavia, via Bassi 21, I-27100 Pavia, Italy
[4] Department of Geological Sciences, University of Manitoba, Winnipeg, MB, R3T 2N2, Canada

[*Received 24 November 2015; Accepted 25 May 2016; Associate Editor: Ian Graham*]

ABSTRACT

New chemical (EMP, SIMS) and structural data are reported for a suite of crystals of oxo-mangani-leakeite and mangano-mangani-ungarettiite from their common type locality, the Hoskins mine (New South Wales, Australia). Notwithstanding the low OH content, FTIR analysis of selected samples has provided considerable information on short-range order in these Mn^{3+}-rich amphiboles, and shows that Li is associated with occupied *A* sites and is linked to the oxo-component at the O(3) site. Comparative analysis of all available data allows us to: (1) further improve our understanding of the crystal-chemistry of these very peculiar compositions of the oxo-amphibole group; and (2) calculate reliable site-populations. The proposed limited compositional variability has been confirmed. The two amphiboles have completely different arrangements of $^{C}R^{3+}$ cations. In oxo-mangani-leakeites, those $^{C}R^{3+}$ cations related to the oxo-component occur at the *M*(1) site, whereas those $^{C}R^{3+}$ cations related to the leakeite charge-arrangement occur at the *M*(2) site. In mangano-mangani-ungarettiite, all $^{C}R^{3+}$ cations order at the *M*(1) and *M*(3) sites, and local bond-valence requirements are satisfied by the presence of Mn^{3+}, which assumes a strongly distorted coordination due to its degenerate e_g electronic state. Therefore, the inverse patterns observed for both cation-ordering and deformation of the octahedra are incompatible with solid-solution between these two species that coexist at the Hoskins mine.

Keywords: amphibole, mangano-mangani-ungarettiite, oxo-mangani-leakeite, structure refinement, FTIR spectroscopy.

Introduction

The recent discovery and characterization of oxo-mangani-leakeite, ideally $^{A}Na\ ^{B}Na_2\ ^{C}(Mn^{3+}_4Li)\ ^{T}Si_8O_{22}\ ^{W}O_2$, from the Hoskins mine, Australia (IMA-CNMNC 2015-035; Oberti *et al.,* 2016*a*), allows us to further investigate two intriguing issues in amphibole crystal-chemistry: [1] the constraints on the incorporation of Li in oxo amphiboles; and [2] the possibility of solid-solution between oxo-mangani-leakeite and mangano-mangani-ungarettiite, $^{A}Na^{B}Na_2{}^{C}(Mn^{2+}_2Mn^{3+}_3)^{T}Si_8O_{22}{}^{W}O_2$, the other oxo amphibole occurring at the Hoskins mine (Ashley, 1986, 1989; Hawthorne *et al.*, 1995). Mangano-mangani-ungarettiite (redefined after Hawthorne *et al.*, 2012) has so far been found only at the Hoskins mine (Hawthorne *et al.*, 1995; Kawachi *et al.*, 2002; this work) and very recently at Bellerberg, Eifel region (work in progress), where it is close to end-member composition. Based on the results of structure refinement, Hawthorne *et al.* (1995) suggested that this feature derives from the

*E-mail: oberti@crystal.unipv.it
https://doi.org/10.1180/minmag.2016.080.124

TABLE 1. A list of the samples relevant to this work (listed by decreasing ^{C}Li contents).

Sample code	CNR-IGG code	Assemblage	Reference
820239	1087	quartz-free	Oberti *et al.*, 2016*a*
820236	1086	quartz-free	Ashley, 1986; this work
12735	1145		this work
820607	1089	quartz-free	this work; *cf.* U2 in Hawthorne *et al.*, 1995
820994	1146	quartz-rich	this work
820240	1135	quartz-rich	U1, Hawthorne *et al.*, 1995

unique ordering of C cations, where the $^{C}R^{3+}$ cations related to the basic eckermannite charge-arrangement occur at the *M*(1) and *M*(3) sites, together with those $^{C}R^{3+}$ cations related to the oxo component. In all ^{W}(OH,F,Cl) amphiboles examined so far, $^{C}R^{3+}$ cations order at the *M*(2) site with one exception: disorder of ^{C}Al occurs between the *M*(2) and *M*(3) sites where Mg/(Mg+Fe^{2+}) is high and/or the *T* of crystallization is above 800°C (Oberti *et al.*, 2007). The pattern of order in mangano-mangani-ungarettiite results in: [1] a strongly elongated and distorted *M*(2) octahedron (octahedral angular variance (Robinson *et al.*, 1971), OAV: 94.2°[2]; *cf.* Table 4); and [2] *M*(1) and *M*(3) polyhedra approaching a [4+2] configuration (OAV: 48.8 and 26.6°[2]) due to the Jahn-Teller distortion typical of $^{[6]}Mn^{3+}$ (Hawthorne *et al.*, 1995).

Many of the rock samples from the Hoskins mine studied by Ashley (1986, 1989) contain amphiboles with significant Li content, another component of amphibole compositional space that is proving to be more common than previously expected. Here, we present a systematic electron-microprobe (EMP), Secondary Ion Mass Spectrometry (SIMS), single-crystal structure refinement (SREF) and Fourier-transform infrared (FTIR) investigation of selected samples provided some years ago by Paul M. Ashley and more recently by Renato and Adriana Pagano. This study has allowed us to characterize compositions and patterns of cation order in oxo-mangani-leakeites with variable Li and oxo contents (up to the border with 'mangani-leakeite', where quote marks indicate that this species has not been characterized and approved by the Commission on New Minerals, Nomenclature and Classification (CNMNC) of the International Mineralogical Association (IMA)), and to confirm previous indications related to the crystal-chemical constraints on the composition of mangano-mangani-ungarettiite.

Samples studied

All samples studied in this work occur in manganese silicate and oxide rocks from the abandoned Hoskins mine, a Mn deposit 3 km west of Grenfell, Forbes Co, New South Wales, Australia (Australian Map Grid Reference 8530-039487). The locality had been studied by Ashley (1986, 1989). Information relevant to parageneses including amphiboles, which occur in rock-forming amounts in scattered samples collected from the old mine dumps, is summarized in Hawthorne *et al.* (1995), who distinguished between "two different assemblages: (1) a reduced assemblage containing rhodonite, tephroite, hausmannite, garnet (spessartine-grossular-andradite-calderite), calcium manganese barium carbonates, quartz, Mn-bearing magnetite, Mn-rich chlorite, caryopilite, barite and pyrite; and (2) an oxidized assemblage containing Mn-rich alkali amphiboles (previously indicated as "leakeite", "Mn-bearing leakeite", manganoan katophorite and manganoan arfvedsonite), clinopyroxenes ranging from namansilite (Kalinin *et al.*, 1992) to aegirine, manganoan pectolite–serandite, braunite, norrishite (Eggleton and Ashley, 1989; Tyrna and Guggenheim, 1991), calcium and barium carbonates, quartz, albite, potassium feldspar, Mn-bearing sugilite and barite".

Oxidized assemblages are commonly foliated and laminated, and may be either quartz-free (amphibole, clinopyroxene, braunite, norrishite and manganoan pectolite–serandite, with minor alkali feldspars, carbonate and barite) or quartz-rich, with subordinate but variable amounts of amphibole and clinopyroxene, and minor serandite, sugilite, norrishite and carbonate (Eggleton and Ashley, 1989). Oxo-mangani-leakeite with slightly variable Li content has been found in two specimens from quartz-free assemblages (820236:

https://doi.org/10.1180/minmag.2016.080.124 Published online by Cambridge University Press

crystal 1086; 820239: crystal 1087, Oberti *et al.*, 2016*a*) and in a specimen (crystal 1145) which has the code 12735 in the mineral collection of Renato and Adriana Pagano (Cinisello Balsamo, Milano, Italy). Hence, specimens 820236 and 12735 should be considered as co-types for oxo-mangano-leakeite. Mangano-mangani-ungarettiite has been found in both quartz-free (sample 820607: crystal 1089) and quartz-rich assemblages (sample 820240: crystal 1135; sample 820994: crystal 1146). A summary of the samples studied is reported in Table 1. The crystal codes are those used in the CNR-IGG crystal-chemical database for amphiboles.

Data collection and refinement

X-ray diffraction (XRD) analysis was performed with a Philips PW1100 4-circle diffractometer (Mo$K\alpha$ radiation) for crystals 1086, 1089 and 1146. Two monoclinic equivalents were collected in the 2θ range 4–60°; corrections for absorption (ψ-scan method, North *et al.*, 1968) and for Lorentz and polarization effects were applied and the collected data were merged to obtain datasets of unique reflections. Unit-cell parameters were calculated from least-squares refinement of the d* values obtained for 60 rows of the reciprocal lattice by measuring the centre of gravity of each reflection and of its antireflection in the 2θ range –70–+70°. For crystal 1145, diffraction data were collected in the 2θ range 2–60° with a Bruker-AXS CCD diffractometer, with graphite-monochromatized Mo$K\alpha$ X-radiation ($\lambda = 0.7107$ Å). Omega-rotation frames (scan width 0.3°, scan time 20 s, sample-to-detector distance 50 mm) were processed with the *SAINT* software (Bruker, 2003) and intensities were corrected for Lorentz and polarization effects; absorption effects were empirically evaluated by the *SADABS* software (Sheldrick, 1996) and an absorption correction was applied to the data. The 7682 collected reflections were reduced to 1298 unique reflections (mean redundancy ≈ 6), and accurate unit-cell dimensions were calculated by least-squares refinement of the positions of 4311 independent reflections with $I_o > 10\ \sigma I$ in the θ range 2–35°.

Only the reflections with $I_o > 3\ \sigma I$ were considered as observed during unweighted full-matrix least-squares refinement on F done with an extensively modified version of the program *ORFLS* (Busing *et al.*, 1962) which is able to deal with complex solid-solutions (Cannillo *et al.*, 1983). Scattering curves for fully ionized chemical species were used at sites where chemical substitutions occur; neutral *vs*. ionized scattering curves were used at the T and anion sites. No constraint related to the chemical analysis was used. The absence of residual electron-density along the **b** direction at ~0.40 Å from the $M(4)$ site (i.e. at the $M(4')$ site) indicates the absence of significant amounts of the smaller B cations (e.g. Li^{+}, Fe^{2+}, Mg^{2+}) at this site.

Crystallographic data for holotype oxo-mangani-leakeite from the Hoskins mine (sample 1087) have been reported in Oberti *et al.* (2016*a*) and those for holotype mangano-mangani-ungarettiite from the same locality (sample 1135) have been given in Hawthorne *et al.* (1995). For these and the other samples, crystallographic details and agreement factors are listed in Table 2; refined coordinates, atom-displacement parameters, and selected bond lengths and angles are reported in Tables 3, 3*b* (deposited with the Principal Editor of *Mineralogical Magazine* and available from http://www.minersoc.org/pages/e_journals/dep_mat_mm.html) and Table 4. The crystallographic information files (cif) with embedded observed structure factors for the samples studied in this work have also been deposited with the Principal Editor and are available from http://www.minersoc.org/pages/e_journals/dep_mat_mm.html.

EMP and SIMS analysis

All new chemical analyses reported in this work were undertaken on the crystals used for the structure refinements. Electron-microprobe (EMP) analyses were carried out with a Cameca SX-100 electron microprobe (wavelength-dispersive spectroscopy mode, 15 kV, 20 nA, counting time 20 s, 1 μm beam diameter). The following standards and crystals were used for $K\alpha$ X-ray lines: Si: diopside, TAP; Ca: diopside, LPET; Ti: titanite, LPET; Cr: chromite, LPET; Fe: fayalite, LLiF; Mn: spessartine, LLiF; Mg: forsterite, LTAP; Al, andalusite, TAP; K: orthoclase, LPET; Na: albite, TAP; F: fluoro-riebeckite, LTAP; Zn: gahnite, LLiF; Ni: pentlandite (LLiF); Cr and Cl contents were below detection limits. Li and H_2O were analysed on crystals 1086 (820236), 1087 (820239), 1089 (820607) and 1135 (820240) by Secondary Ion Mass Spectrometry (SIMS) using a Cameca IMS 4f with an $^{16}O^{-}$ primary beam focused on the target surface to form spot of ~15 μm in diameter. Beam current was 10 nA and the energy-filtering

https://doi.org/10.1180/minmag.2016.080.124 Published online by Cambridge University Press

TABLE 2. Unit-cell parameters (Å, °, Å^3) and crystallographic details for the samples first described in this work, oxo-mangani-leakeite (820236 and 12735) and mangano-mangani-ungarettiite (820607 and 820994). Holotype oxo-mangani-leakeite (820239; Oberti *et al.*, 2016*a*) and mangano-mangani-ungarettiite U1 (820240; Hawthorne *et al.*, 1995) are listed for comparison.

	Oxo-mangani-leakeite			Mangano-mangani-ungarettiite		
	820239	820236	12735	820607	820994	820240
a	9.875(5)	9.868(4)	9.845(1)	9.885(5)	9.874(5)	9.889(4)
b	17.873(9)	17.877(10)	17.821(1)	18.031(6)	17.976(13)	18.033(7)
c	5.295(2)	5.291(3)	5.300(1)	5.294(2)	5.298(3)	5.296(2)
β	104.74(3)	104.54(3)	104.97(1)	105.08(2)	105.09(4)	105.08(2)
V	903.9(7)	903.5(8)	898.3(1)	911.1(7)	907.9(10)	911.9(6)
θ range	2–30	2–30	2–30	2–30	2–30	2–30
Space group	*C*2/*m*	*C*2/*m*	*C*2/*m*	*C*2/*m*	*C*2/*m*	*C*2/*m*
R_{symn} %	3.1	2.2	1.7	2.0	2.1	2.2
R_{obs} %	2.01	1.86	2.51	1.79	2.65	1.78
R_{all} %	6.47	5.04	2.83	4.22	4.80	4.20
# all	1372	1369	1298	1379	1376	1384
# obs	769	934	1282	954	969	938

technique was used to eliminate any possible molecular interference and to reduce matrix effects. Secondary positive-ion currents were measured at masses 1 (H), 7 (Li) and 30 (Si, used as the reference element) and corrected for isotopic abundances. The results were put on a quantitative basis using empirical calibration curves based on well-characterized standards (silicates and glasses). Precision and accuracy are better than ±10%. Further analytical details are reported by Oberti *et al.* (2003). For crystal 1145 (12735), Li was estimated based on SREF results (Oberti *et al.*, 2003), and H_2O was estimated by assuming complete oxidation of both Fe and Mn, by analogy to what was observed in the other crystals of oxo-mangani-leakeite. Crystal 1146 (820994) was lost during preparation of the EMP mount; as a test of the procedure, its crystal-chemical features were assessed based on the results of the structure refinement and FTIR analysis. Analytical data and unit formulae are given in Table 5. Note that in the case of holotype mangano-mangani-ungarettiite (samples 820994 and 820240 characterized by Hawthorne *et al.*, 1995), SIMS analyses were undertaken on a crystal different from that used for structure refinement.

FTIR analysis

Fourier-Transform Infrared spectroscopy was performed on: (1) a crystal from sample 820239 (holotype oxo-mangani-leakeite; Oberti *et al.*, 2016*a*); (2) a crystal from sample 820607 (holotype mangano-mangani-ungarettiite; *cf.* U2 in Hawthorne *et al.* (1995) and 1089 in this work); (3) a crystal from sample 820994. The goal was both to validate and cross-calibrate SIMS analysis for H_2O and to understand details of the local order of C cations in the different compositions. All the crystals used for FTIR analysis had been checked by XRD to verify their homogeneity with the crystals used for SREF and for EMP and SIMS analysis.

Spectra were collected in transmission mode on very small, randomly oriented crystal fragments, using a Nicolet NicPlan microscope at University Roma Tre, equipped with an MCT detector. The microscope was attached to a Magna 760 optical bench, equipped with a KBr beamsplitter and a globar IR source.

Results and discussion

FTIR

Several single spots were collected for each crystal; selected data are shown in Fig. 1. All spectra recorded on mangano-mangani-ungarettiite 820994 showed that this amphibole is completely anhydrous. Those recorded for oxo-mangani-leakeite 820239 and for mangano-mangani-ungarettiite 820607 confirm the presence of small

https://doi.org/10.1180/minmag.2016.080.124 Published online by Cambridge University Press

TABLE 3. Refined site-scattering values (ss), atom coordinates and equivalent isotropic atomic displacement parameters (B_{eq}) in oxo-mangani-leakeite (820236 and 12735) and mangano-mangani-ungarettiite (820607 and 820994) first described in this work.

Atom	ss (epfu)	*x/a*	*y/b*	*z/c*	B_{eq} (Å^2)
820236 (1086)					
O(1)		0.1124(2)	0.08880(10)	0.2137(3)	0.86(4)
O(2)		0.1186(2)	0.16712(10)	0.7232(4)	0.90(4)
O(3)		0.1072(3)	0	0.7035(5)	1.11(6)
O(4)		0.3596(2)	0.24974(10)	0.7991(4)	1.06(4)
O(5)		0.3482(2)	0.12773(9)	0.0824(4)	0.89(4)
O(6)		0.3442(2)	0.11875(9)	0.5834(4)	0.91(4)
O(7)		0.3361(3)	0	0.2967(5)	1.09(6)
T(1)		0.27928(7)	0.08586(3)	0.29200(13)	0.56(2)
T(2)		0.28775(7)	0.17068(3)	0.79846(13)	0.53(2)
M(1)	35.61(13)	0	0.08522(4)	$^1/_2$	0.66(2)
M(2)	43.58(13)	0	0.18066(4)	$^1/_2$	0.62(2)
M(3)	9.32(5)	0	0	0	0.53(5)
M(4)	22.6(2)	0	0.27571(8)	$^1/_2$	1.26(4)
A	4.08(3)	0	$^1/_2$	0	2.3(2)
A(*m*)	9.49(8)	0.0407(4)	$^1/_2$	0.0938(8)	2.48(10)
12735 (1145)					
O(1)		0.11319(14)	0.08930(7)	0.2104(3)	0.99(3)
O(2)		0.11863(13)	0.16558(7)	0.7192(3)	0.97(3)
O(3)		0.1056(2)	0	0.7013(4)	1.28(4)
O(4)		0.3590(2)	0.25043(7)	0.8007(3)	1.14(3)
O(5)		0.34982(13)	0.12752(8)	0.0805(3)	0.95(3)
O(6)		0.34638(13)	0.11948(7)	0.5818(3)	0.96(3)
O(7)		0.3379(2)	0	0.2985(4)	1.26(4)
T(1)		0.28118(5)	0.08601(3)	0.29071(9)	0.646(9)
T(2)		0.28879(5)	0.17041(3)	0.79677(9)	0.640(9)
M(1)	41.46(10)	0	0.08364(3)	$^1/_2$	0.796(13)
M(2)	43.14(10)	0	0.17991(2)	$^1/_2$	0.728(10)
M(3)	9.89(4)	0	0	0	0.83(4)
M(4)	22.9(2)	0	0.27480(6)	$^1/_2$	1.49(3)
A	2.74(3)	0	$^1/_2$	0	1.9(2)
A(*m*)	10.79(8)	0.0424(3)	$^1/_2$	0.0957(5)	2.44(7)
820607 (1089)					
O(1)		0.1201(2)	0.08318(9)	0.2087(4)	0.68(4)
O(2)		0.1168(2)	0.15936(9)	0.7082(4)	0.64(4)
O(3)		0.0915(3)	0	0.7186(5)	0.72(5)
O(4)		0.3492(2)	0.24848(10)	0.7902(4)	0.95(4)
O(5)		0.3503(2)	0.12627(10)	0.0713(3)	0.78(4)
O(6)		0.3488(2)	0.11847(10)	0.5755(3)	0.85(4)
O(7)		0.3499(3)	0	0.2939(6)	0.97(6)
T(1)		0.28837(7)	0.08407(3)	0.28595(13)	0.49(2)
T(2)		0.28695(7)	0.16807(3)	0.78618(14)	0.50(2)
M(1)	50.02(10)	0	0.08145(3)	$^1/_2$	0.489(12)
M(2)	47.18(13)	0	0.18341(3)	$^1/_2$	0.59(2)
M(3)	24.12(5)	0	0	0	0.42(4)
M(4)	22.4(2)	0	0.27296(9)	$^1/_2$	1.54(5)
A	2.75(5)	0	$^1/_2$	0	2.5(4)
A(*m*)	6.23(11)	0.0433(11)	$^1/_2$	0.097(2)	2.5(2)
A(2)	3.68(11)	0	0.498(6)	0	4.4(4)

(continued)

https://doi.org/10.1180/minmag.2016.080.124 Published online by Cambridge University Press

TABLE 3. (*contd*.)

Atom	ss (epfu)	*x/a*	*y/b*	*z/c*	B_{eq} (Å^2)
820994 (1146)					
O(1)		0.1191(3)	0.08402(13)	0.2081(5)	0.61(6)
O(2)		0.1170(2)	0.16034(13)	0.7109(5)	0.60(5)
O(3)		0.0929(4)	0	0.7157(7)	0.62(7)
O(4)		0.3503(3)	0.24905(14)	0.7926(5)	0.87(6)
O(5)		0.3507(3)	0.12659(14)	0.0728(5)	0.73(5)
O(6)		0.3486(3)	0.11897(14)	0.5774(5)	0.76(5)
O(7)		0.3489(4)	0	0.2949(7)	0.92(8)
T(1)		0.28762(10)	0.08448(5)	0.2871(2)	0.42(2)
T(2)		0.28713(10)	0.16857(5)	0.7882(2)	0.42(2)
M(1)	50.00	0	0.08177(4)	$^1/_2$	0.52(2)
M(2)	44.6(2)	0	0.18267(5)	$^1/_2$	0.57(2)
M(3)	25.00	0	0	0	0.77(2)
M(4)	22.67(13)	0	0.27356(12)	$^1/_2$	1.41(5)
A(*m*)	8.9(2)	0.0367(8)	$^1/_2$	0.073(2)	3.8(3)
A(2)	4.6(2)	0	0.4968(4)	0	5.3(5)

epfu – electrons per formula unit.

amounts of OH, in accord with EMP + SIMS + SREF analyses (Table 5). It is worth noting that crystal size prevented us from obtaining doubly polished sections with defined and measurable thickness; hence, the data presented in Fig. 1 cannot be considered as fully quantitative. On the other hand, the spectra reported in Fig. 1 show that the method is effective in analysing very small amounts of OH, as is the case for sample 820207, which gave a very well-defined weak doublet at 3648–3660 cm^{-1} although it has a very low OH content (0.08 atoms per formula unit (apfu), Table 5).

According to the SIMS results, sample 820607 has a very low but significant Li content (0.03 apfu). We have examined the possible local arrangements of cations in order to understand whether there is local order involving $^{M(3)}Li^+$ ions and $^{O(3)}OH^-$ groups. The interpretation of the spectra of Fig. 1 in terms of short-range arrangements is not straightforward, because several cation and anion combinations are locally possible in these amphiboles. The spectrum of sample 820607 can be used as a starting point, because the composition of the *M*(1,3) sites is relatively simple (Table 6). A tentative decomposition of the spectrum following the method of Della Ventura *et al.* (1999, 2003) and Hawthorne *et al.* (2000) is given in Fig. 2*a*. Four components can be resolved under the most intense doublet, centred at 3674, 3660, 3647 and 3635 cm^{-1}, respectively. At higher frequencies, another weak component can be resolved at 3704 cm^{-1}; the remaining signal is noise. There are several considerations which may help in interpreting the spectrum of 820607. First, the fitted components are rather sharp (full width at half maximum of 12–13 cm^{-1}), and have a frequency separation of ~13 cm^{-1}. These features are typical of two divalent cations distributed over the three OH-coordinated *M*(1)*M*(1)*M*(3) octahedra (e.g. Della Ventura *et al.*, 1996, 1997, Reece *et al.*, 2002). Based on the chemical analysis (Table 5), most of the *M*(1,3) sites are occupied by Mn^{3+} ions, and hence ~95% of the local *M*(1)*M*(1)*M*(3) trimers must be $Mn^{3+}Mn^{3+}Mg$. These arrangements are expected to coordinate 2 O^{2-} ions, and hence are invisible to IR analysis. This being the case, the 5% residual arrangements involving Mg, Mn^{2+} and Li over the *M*(1,3) sites must be bonded to the ~5% remaining OH groups in the crystal. Given the wavenumbers measured, these arrangements are associated locally with vacant *A* sites (Della Ventura *et al.*, 2003, Hawthorne and Della Ventura, 2007). Arrangements with $Mn^{3+}MgMg$ can be excluded as they would be associated with much broader components and shifted to frequencies lower than those observed in Fig. 2. Therefore, the quartet of bands at 3674, 3660, 3647 and 3635 cm^{-1} can be assigned, respectively, to OH bonded to MgMgMg, $MgMgMn^{2+}$, $MgMn^{2+}Mn^{2}$ and $Mn^{2+}Mn^{2+}Mn^{2+}$ arrangements and directed toward a vacant *A* site. The observed frequencies are consistent with those reported by Reece *et al.*

https://doi.org/10.1180/minmag.2016.080.124 Published online by Cambridge University Press

TABLE 4. Selected interatomic distances (Å) and angles (°) and distortion parameters, in oxo-mangani-leakeite (820236 and 12735) and mangano-mangani-ungarettiite (820607 and 820994). Holotype oxo-mangani-leakeite (820239; Oberti *et al.*, 2016*a*) and mangano-mangani-ungarettiite U1 (820240; Hawthorne *et al.*, 1995) are listed for comparison.

	Oxo-mangani-leakeite			Mangano-mangani-ungarettiite		
	820239	820236	12735	820607	820994	820240
T(1)–O(1)	1.599(3)	1.595(2)	1.5988(14)	1.607(2)	1.607(3)	1.607(2)
T(1)–O(5)	1.624(2)	1.622(2)	1.6232(14)	1.615(2)	1.618(3)	1.615(2)
T(1)–O(6)	1.623(3)	1.624(2)	1.6236(13)	1.617(2)	1.622(3)	1.615(2)
T(1)–O(7)	1.633(2)	1.6321(13)	1.6284(8)	1.6301(13)	1.631(2)	1.6307(11)
<*T*(1)–O>	1.620	1.618	1.618	1.617	1.620	1.617
TQE	1.0032	1.0030	1.0030	1.0025	1.0026	1.0024
TAV	13.13	12.63	12.23	9.93	10.43	9.78
T(2)–O(2)	1.615(2)	1.617(2)	1.6207(13)	1.631(2)	1.629(3)	1.631(2)
T(2)–O(4)	1.579(2)	1.581(2)	1.5826(14)	1.573(2)	1.573(3)	1.571(2)
T(2)–O(5)	1.654(3)	1.659(2)	1.6551(14)	1.657(2)	1.656(3)	1.659(2)
T(2)–O(6)	1.667(2)	1.669(2)	1.6667(14)	1.665(2)	1.662(3)	1.664(2)
<*T*(2)–O>	1.629	1.631	1.631	1.632	1.630	1.631
TQE	1.0049	1.0053	1.0050	1.0050	1.0050	1.0048
TAV	21.17	22.67	21.73	21.22	21.21	20.15
M(1)–O(1) ×2	2.107(3)	2.091(2)	2.1195(13)	2.177(2)	2.174(3)	2.184(2)
M(1)–O(2) ×2	2.040(2)	2.053(2)	2.0358(14)	1.965(2)	1.976(3)	1.968(2)
M(1)–O(3) ×2	2.008(2)	2.007(2)	1.9665(13)	1.941(2)	1.940(3)	1.941(2)
<*M*(1)–O>	2.052	2.050	2.041	2.028	2.030	2.031
Δ	4.04	2.80	9.40	27.32	25.64	28.74
OAV	28.17	30.36	32.36	48.09	46.54	48.82
M(2)–O(1) ×2	2.134(3)	2.139(2)	2.1095(14)	2.283(2)	2.251(3)	2.282(2)
M(2)–O(2) ×2	2.129(2)	2.106(2)	2.1315(13)	2.199(2)	2.183(3)	2.199(2)
M(2)–O(4) ×2	1.964(3)	1.965(2)	1.9561(14)	2.026(2)	2.013(3)	2.029(2)
<*M*(2)–O>	2.076	2.070	2.066	2.169	2.149	2.170
Δ	14.46	13.35	14.28	24.43	21.64	23.58
OAV	48.35	46.78	46.41	93.81	85.07	94.15
M(3)–O(1) ×4	2.093(2)	2.097(2)	2.0918(13)	2.049(2)	2.050(3)	2.047(2)
M(3)–O(3) ×2	2.110(4)	2.101(3)	2.107(2)	1.934(3)	1.957(4)	1.933(2)
<*M*(3)–O>	2.099	2.098	2.097	2.010	2.019	2.009
Δ	0.16	0.01	0.11	7.25	4.75	7.11
OAV	50.83	52.21	55.02	27.47	30.61	26.60

(continued)

TABLE 4. (*contd.*)

	Oxo-mangani-leakeite			Mangano-mangani-ungarettiite		
	820239	820236	12735	820607	820994	820240
M(4)–O(2) ×2	2.417(3)	2.416(2)	2.408(2)	2.466(2)	2.460(3)	2.468(2)
M(4)–O(4) ×2	2.402(3)	2.394(2)	2.4111(14)	2.434(2)	2.438(3)	2.438(2)
M(4)–O(5) ×2	2.915(3)	2.906(2)	2.909(2)	2.982(2)	2.963(3)	2.982(2)
M(4)–O(6) ×2	2.541(3)	2.542(2)	2.523(2)	2.557(2)	2.541(3)	2.557(2)
<*M*(4)–O>	2.569	2.565	2.563	2.610	2.601	2.611
A–O(5) ×4	2.819(2)	2.824(2)	2.8031(14)	2.794(2)	–	–
A–O(6) ×4	3.163(2)	3.167(2)	3.1626(13)	3.178(2)	–	–
A–O(7) ×2	2.518(4)	2.521(3)	2.520(2)	2.413(3)	–	–
<*A*–O>	2.896	2.901	2.890	2.871	–	–
A(2)–O(5) x2	–	–	–	2.77(9)	2.75(6)	2.613(8)
A(2)–O(6) x2	–	–	–	3.16(8)	3.14(5)	3.033(6)
A(2)–O(7) x2	–	–	–	2.413(3)	2.426(4)	2.420(3)
<*A*(2)–O>	–	–	–	2.78	2.77	2.689
A(*m*)–O(5) ×2	2.972(6)	2.961(5)	2.947(3)	2.950(8)	2.924(7)	2.921(4)
A(*m*)–O(5) ×2	2.784(5)	2.793(4)	2.770(3)	2.752(7)	2.732(5)	2.745(4)
A(*m*)–O(6) ×2	2.758(6)	2.782(4)	2.773(3)	2.782(6)	2.862(8)	2.855(6)
A(*m*)–O(7)	2.519(9)	2.513(7)	2.515(5)	2.403(13)	2.439(9)	2.402(6)
A(*m*)–O(7)	3.118(9)	3.148(7)	3.122(4)	3.120(10)	3.243(11)	3.224(9)
A(*m*)–O(7)	2.651(10)	2.648(7)	2.650(5)	2.558(12)	2.496(9)	2.507(6)
<*A*(*m*)–O>	2.813	2.820	2.807	2.783	2.801	2.797
M(1) –*M*(2)	3.150(2)	3.148(2)	3.1570(4)	3.2229(10)	3.211(2)	3.2245(4)
O(5)–O(6)–O(5)	173.03(12)	172.86(11)	173.65(8)	173.91(11)	174.0(2)	173.92(11)
O(6)–O(7)–O(6)	109.6(2)	109.56(13)	110.31(9)	110.09(13)	110.0(2)	109.99(12)
T(1)–O(5)–*T*(2)	136.1(2)	135.72(12)	135.75(8)	137.12(12)	136.7(2)	137.13(12)
T(1)–O(6)–*T*(2)	136.6(2)	136.84(12)	136.80(9)	137.05(12)	137.1(2)	137.20(11)
T(1)–O(7)–*T*(1)	140.2(2)	140.3(2)	140.55(14)	136.9(2)	137.2(3)	136.7(2)

Angular variance (AV, °^{2}) and quadratic elongation (QE) are defined for tetrahedra (T) and octahedra (O) as in Robinson *et al.* (1971); Δ, the mean-square relative deviation from the average, is calculated as in Brown and Shannon (1973).

TABLE 5. Microchemical data (from EMP, SIMS and SREF) and crystal-chemical formulae for the samples of this work and for the two holotype reference samples.

	Oxo-mangani-leakeite			Mangano-mangani-ungarettiite	
	820239[§]	820236	12735	820607	820240[§§]
SiO_2	53.53(63)	54.20(71)	54.33(51)	50.45(78)	50.66(44)
TiO_2	0.28(5)	0.34(4)	0.62(6)	n.d	n.d.
Al_2O_3	0.29(7)	0.34(7)	0.17(4)	0.33(5)	n.d.
FeO	0.00	0.00	0.00	0.00	0.00
Fe_2O_3	3.91(12)	5.50(15)	3.79(13)	0.54(4)	0.50(7)
Mn_2O_3	20.46(24)	15.52(21)	21.73(19)	23.04(27)	24.35(26)
MnO	0.00	0.00	0.00	12.69(15)	12.42(14)
MgO	7.20(8)	9.08(14)	6.85(9)	1.52(7)	1.46(6)
ZnO	0.13(3)	0.11(4)	n.d	0.02(2)	n.d.
Li_2O	0.96	0.94	0.89	0.04	0.02
NiO	0.06(3)	0.07(3)	0.17(5)	0.04(2)	n.d.
CaO	0.36(9)	0.60(12)	0.24(5)	0.19(4)	0.18(4)
Na_2O	8.96(7)	8.70(8)	9.31(9)	9.10(8)	9.13(7)
K_2O	1.90(5)	1.91(8)	1.50(9)	0.76(8)	0.76(7)
H_2O	0.64	0.99	0.49	0.08	0.00
Total	98.68	98.30	100.09	98.80	99.48
Si	7.98	8.00	8.00	8.00	8.00
Al	0.02	0.00	0.00	0.00	0.00
ΣT	8.00	8.00	8.00	8.00	8.00
Al	0.03	0.06	0.03	0.06	0.00
Fe^{3+}	0.44	0.61	0.42	0.06	0.06
Mn^{3+}	2.32	1.74	2.44	2.78	2.93
Ti	0.03	0.04	0.07	0.00	0.00
Zn	0.01	0.01	0.00	0.00	0.00
Ni	<0.01	<0.01	0.02	<0.01	0.00
Mg	1.60	2.00	1.50	0.36	0.34
Mn^{2+}	–	–	–	1.70	1.66
Li	0.58	0.55	0.52	0.03	0.01
ΣC	5.01	5.01	5.00	5.00	5.00
Li	0.00	0.01	0.00	0.00	0.00
Ca	0.06	0.09	0.04	0.03	0.03
Na	1.94	1.90	1.96	1.97	1.97
ΣB	2.00	2.00	2.00	2.00	2.00
Na	0.65	0.59	0.70	0.83	0.83
K	0.36	0.36	0.28	0.15	0.15
ΣA	1.01	0.95	0.98	0.98	0.98
OH	0.66	0.98	0.48	0.08	0.00
O^{2-}	1.34	1.02	1.52	1.92	2.00
ΣW	2.00	2.00	2.00	2.00	2.00

n.d.: not detected.
*Calculated; formula normalized to 24 (O, F, Cl, OH) atoms per formula unit; [§]Oberti *et al.*, (2016*a*); [§§]sample U1, Hawthorne *et al.* (1995).

https://doi.org/10.1180/minmag.2016.080.124 Published online by Cambridge University Press

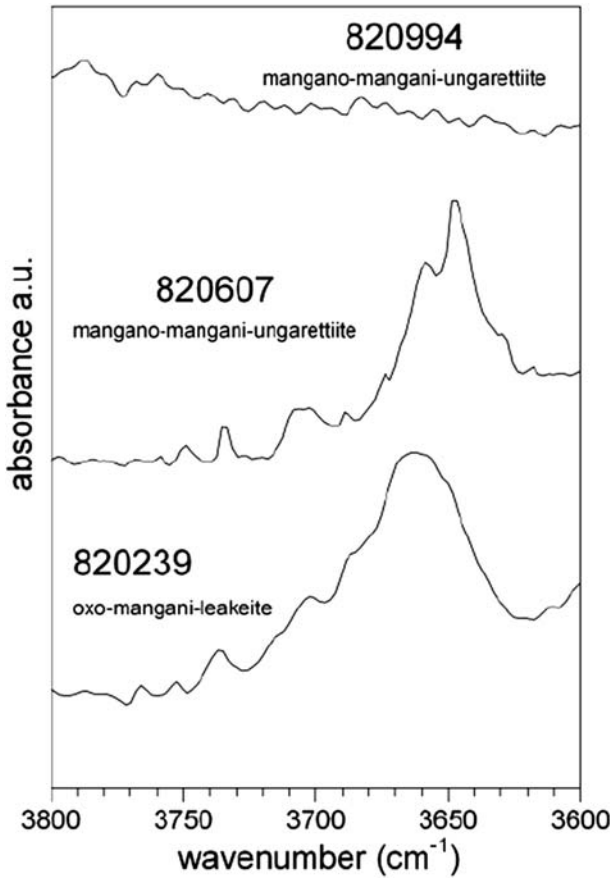

FIG. 1. FTIR spectra for the studied samples in the fundamental OH-stretching region

(2002) for synthetic $^{C}(Mg,Mn)^{2+}$ amphiboles. Assignment of the weak component at 3704 cm^{-1} is more problematic. This wavenumber is very close to that of the main band of pargasite (Robert *et al.*, 1996, Della Ventura *et al.*, 1998, 1999), where the proton is involved in a weak interaction with the O(7) oxygen bridging *T*(1)–O(7)–*T*(1) linkages (Hawthorne *et al.*, 1996*a*,*b*; Della Ventura *et al.*, 1999). Our optimum site-populations (Table 5) do not assign any Al to the *T*(1) site; however, considering the very low intensity of the 3704 cm^{-1} component, the presence of trace Al at *T* (1) cannot be discounted.

The interpretation of the spectrum of sample 820239 (Fig. 2*b*) is even less straightforward, because the *M*(1–3) composition is more complicated (Table 6). Indeed, the component bands are much broader than those of sample 820607, indicating significant cation disorder (e.g. Hawthorne *et al.*, 1997, Hawthorne and Della Ventura, 2007) and hence a larger number of chemically and geometrically different arrangements. According to the unit formula of sample 820239, all possible cation arrangements must be associated with an *A* site fully occupied by Na and K, a feature that significantly affects the IR spectrum in terms of both band position and width (e.g. Hawthorne *et al.*, 1997; Gottschalk and Andrut, 1998; Della Ventura *et al.*, 2003).

The main band at 3670 cm^{-1} in the spectrum is shifted 60 cm^{-1} towards lower wavenumbers with respect to a hypothetical MgMgMg–OH–Na arrangement, which can be taken as the reference point of this discussion because Mg is the only divalent cation occurring at *M*(1,3). Based on the proposed site-populations, the 3670 cm^{-1} band can be assigned to an Mn^{3+}MgMg–OH–^{A}Na arrangement. Data from the literature (see Hawthorne and Della Ventura, 2007 for a compilation) show that the shift due to a trivalent C cation is 30 cm^{-1}

https://doi.org/10.1180/minmag.2016.080.124 Published online by Cambridge University Press

TABLE 6. Site populations calculated based on all the information made available from this work.

		Site scattering (epfu)		Mean bond lengths (Å)	
	Site population (apfu)	Measured	Calculated*	Measured	Calculated*
820239 (1087) oxo-mangani-leakeite					
T(1)	3.98 Si + 0.02 Al			1.620	1.620
T(2)	4.00 Si				
M(1)	0.84 Mg + 1.13 Mn^{3+} + 0.03 Ti^{4+}	39.04	38.99	2.052	2.046
M(2)	0.48 Mg + 0.03 Al + 0.44 Fe^{3+} + 1.04 Mn^{3+} + 0.01 Zn	45.94	43.89	2.076	2.047
M(3)	0.27 Mg + 0.15 Mn^{3+} + 0.58 Li	8.99	8.73	2.099	2.093
C cations		93.97	91.60		
B cations	1.94 Na + 0.06 Ca	22.60	22.54		
A cations	0.64 Na + 0.36 K	13.81	13.88		
W anions	1.31 O^{2-} + 0.69 OH				
820236 (1086) oxo-mangani-leakeite					
T(1)	4.00 Si			1.618	1.620
T(2)	4.00 Si				
M(1)	1.12 Mg + 0.84 Mn^{3+} + 0.04 Ti^{4+}	35.61	35.32	2.050	2.053
M(2)	0.58 Mg + 0.06 Al + 0.61 Fe^{3+} + 0.75 Mn^{3+} + 0.01 Zn	43.58	42.65	2.070	2.048
M(3)	0.30 Mg + 0.15 Mn^{3+} + 0.55 Li	9.32	9.00	2.098	2.092
C cations		88.51	86.97		
B cations	1.90 Na + 0.09 Ca + 0.01 Li	22.62	22.73		
A cations	0.59 Na + 0.36 K	13.57	13.34		
W anions	1.02 O^{2-} + 0.98 OH				
12735 (1145) oxo-mangani-leakeite					
T(1)	4.00 Si			1.618	1.620
T(2)	4.00 Si				
M(1)	0.66 Mg + 1.27 Mn^{3+} + 0.07Ti^{4+}	41.46	41.21	2.041	2.040
M(2)	0.54 Mg + 0.03 Al + 0.42 Fe^{3+} + 0.99 Mn^{3+} + 0.02 Ni	43.14	43.10	2.066	2.038
M(3)	0.30 Mg + 0.18 Mn^{3+} + 0.52 Li	9.89	9.66	2.097	2.089
C cations		94.49	93.97		
B cations	1.96 Na + 0.04 Ca	22.91	22.36		
A cations	0.70 Na + 0.28 K	13.53	13.02		
W anions	1.52 O^{2-} + 0.48 OH				

(continued)

TABLE 6. (*contd.*)

	Site population (apfu)	Site scattering (epfu)		Mean bond lengths (Å)	
		Measured	Calculated*	Measured	Calculated*
820607 (1089) mangano-mangani-ungarettiite					
T(1)	4.00 Si			1.617	1.620
T(2)	4.00 Si				
M(1)	0.04 Mg + 0.04 Mn^{2+} + 1.86 Mn^{3+} + 0.06 Fe^{3+}	50.02	49.54	2.028	2.029
M(2)	0.30 Mg + 0.06 Al + 1.64 Mn^{2+}	47.18	45.38	2.169	2.151
M(3)	0.03 Mg + 0.02 Mn^{2+} + 0.92 Mn^{3+} + 0.03 Li	24.12	23.95	2.010	2.032
C cations		121.32	118.87		
B cations	1.97 Na + 0.03 Ca	22.40	22.27		
A cations	0.83 Na + 0.15 K	12.66	11.98		
W anions	1.92 O^{2-} + 0.08 OH				
820994 (1146) mangano-mangani-ungarettiite					
T(1)	4.00 Si			1.617	1.620
T(2)	4.00 Si				
M(1)	2.00 Mn^{3+}	50.00	50.00	2.030	2.025
M(2)	0.42 Mg + 1.58 Mn^{2+}	44.60	44.54	2.149	2.153
M(3)	1.00 Mn^{3+}	25.00	25.00	2.019	2.025
C cations		119.60	119.54		
B cations	2.00 Na	22.67	22.00		
A cations	0.70 Na + 0.30 K	13.41	13.40		
W anions	2.00 O^{2-}				
820240 (1135) mangano-mangani-ungarettiite					
T(1)	4.00 Si			1.617	1.620
T(2)	4.00 Si				
M(1)	2.00 Mn^{3+}	50.02	50.00	2.031	2.025
M(2)	0.22 Mg + 1.78 Mn^{2+}	47.13	47.14	2.170	2.163
M(3)	0.06 Mg + 0.94 Mn^{3+}	24.20	24.22	2.009	2.029
C cations		121.35	121.36		
B cations	1.97 Na + 0.03 Ca	22.23	22.27		
A cations	0.83 Na + 0.15 K	12.16	11.98		
W anions	2.00 O^{2-}				

*Calculated from site populations according to Oberti *et al.* (2016*a*), i.e. using a model which does not take into account peculiar polyhedral distortion.

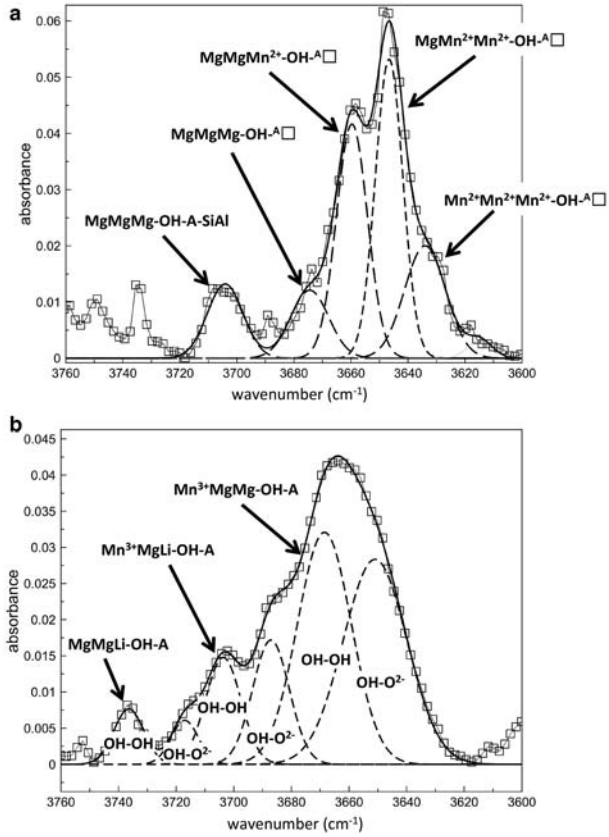

FIG. 2. Decomposition of the FTIR spectra and proposed band assignment for mangano-mangani-ungarettiite 820607 (*upper*) and oxo-mangani-leakeite 820239 (*lower*).

for Al, and ~50 cm^{-1} for Fe^{3+}; hence, a shift of 60 cm^{-1} seems reasonable for Mn^{3+}. The band at 3705 cm^{-1} is shifted upwards by ~35–40 cm^{-1} with respect to the 3670 cm^{-1} band; this shift is compatible only with the presence of ^{C}Li. Hence, the 3705 cm^{-1} component is assigned to the Mn^{3+}MgLi–OH–^{A}Na arrangement. A minor band is resolved at 3738 cm^{-1}, a wavenumber typical of an arrangement with a 5+ aggregate cation charge (Robert *et al.*, 1989); this component can only be assigned to a MgMgLi–OH–^{A}Na arrangement.

The three bands discussed so far (marked with arrows in Fig. 2*b*) are all associated with a second component shifted downward by 20 cm^{-1}. Della Ventura *et al.* (2007) showed that in deprotonated amphiboles, the fundamental OH-stretching band is shifted downwards by 20 cm^{-1} where the OH group is locally facing a deprotonated O(3) site across the *A* cavity. This effect is similar to the case where the O(3) site is occupied by F, which is visible in the IR spectrum only where the *A* site is occupied (Robert *et al.*, 1999). Hence, the second set of bands is assigned to the same arrangements facing a deprotonated O(3) site. Interestingly, the two types of bands have almost the same intensity, implying that the amounts of the two arrangements are the same. Therefore, FTIR analysis does not provide any evidence of Li-oxo avoidance.

Cation ordering, site populations and crystal-chemical issues

The optimum site-populations obtained by integrating the available chemical and crystal-chemical data (plus FTIR information for sample 820607) are shown in Table 6. The ordering pattern and the relaxation scheme proposed for mangano-mangani-ungarettiite by Hawthorne *et al.* (1995) is

https://doi.org/10.1180/minmag.2016.080.124 Published online by Cambridge University Press

confirmed for all samples characterized in the present work, independent of the amount of Mg present, which seems to be the only variable involved, together with the Na/K ratio. As noted in the Introduction, mangano-mangani-ungarettiite is the only amphibole known so far where highly charged cations related to the non-oxo stoichiometry do not order at the *M*(2) site but occur at the *M*(1) and *M*(3) sites together with those involved in the oxo-component. This work also confirms that mangano-mangani-ungarettiite crystals are always very close to end-member composition, and that Mn is an essential constituent to obtain the observed pattern of cation ordering and geometrical distortion because its high spin d^4 configuration implies a strong tendency towards electronic degeneracy in an octahedral ligand field, and hence a strong distortion (as observed in Table 4).

Focusing on the recently characterized oxo-mangani-leakeite, SREF-based site populations for sample 820239 were derived in Oberti *et al.* (2016*a*) based on structure refinement. They show that the highly charged C cations involved in the leakeite stoichiometry are ordered at the *M*(2) site, whereas those involved in the deprotonation process are almost completely ordered at the *M*(1) site (1.13 Mn^{3+} + 0.03 Ti^{4+}), and that only a minor contribution to overall electroneutrality and local charge balance is provided by highly charged cations at the *M*(3) site (0.15 Mn^{3+}). This peculiarity derives from the fact that ^{C}Li orders at the *M*(3) site, and is in accord with the observation that the *M*(3) octahedron has a mean bond distance longer than that calculated based on its site population (2.099 *vs.* 2.093 Å) and is nearly regular in terms of individual bond-lengths, contrary to what is observed in mangano-mangani-ungarettiite, where the *M*(3) octahedron tends toward a [4 + 2] coordination (Table 4). These site populations are in accord with the interpretation of the FTIR spectrum as discussed in the previous section.

The newly characterized crystals of oxo-mangani-leakeite described in this work differ mainly by their Mg content, the restricted Li content of 0.52–0.58 apfu, and the restricted Na content at the *A* site of 0.59–0.70 apfu (at nearly constant *A*-site occupancy). In all samples, there is strong relaxation around the *M*(2) site, which couples with a (weaker) relaxation around the *M*(3) site, hindering the incorporation of trivalent cations. Tait *et al.* (2005) described the only other known Li-bearing oxo-amphibole (mangani-della-venturaite, $^{A}Na^{B}Na_2{}^{C}(MgMn^{3+}_2Ti^{4+}Li)^{T}Si_8O_{22}{}^{W}O_2$, redefined after Hawthorne *et al.*, 2012) and argued that the $^{M(3)}Li$–$^{O(3)}O^{2-}$ avoidance generated by local bond-valence requirements can be overcome solely by the presence of $^{[6]}Mn^{3+}$, where the energetically degenerate e_g electronic state favours spontaneous distortion of the octahedron. As a consequence, $^{M(1)}Mn^{3+}$ ions allow much shorter (and stronger) bonds to O(3) than $^{M(1)}Fe^{3+}$ ions, as is the case for the samples of this work (Table 3). Notably, the observed variation in the *M*(1)–*M*(2) distances is in the expected relation to that of the O^{2-} content (Oberti *et al.*, 2007), confirming that this distance is a sound indication of the oxo-component in amphiboles.

Although coexisting in the same assemblages, oxo-mangani-leakeite and mangano-mangani-ungarettiite have distinct patterns of cation order. A very important point here is that the two patterns of cation order are quite incompatible with each other, both from geometrical and bond-valence points of view. Consequently, extensive solid-solution between these two amphiboles (which would involve the $^{C}Mn^{3+}_{-1}$ $^{C}Li^{+}_{-1} \rightarrow {}^{C}(Mg,Mn)^{2+}_2$ coupled exchange) is not possible, and this conclusion explains the distinct and almost constant compositions described in this work. As a final comment, crystal-chemical investigation of sodium amphiboles is providing increasing evidence for a dominant role of the *M*(1) cations in the heterovalent exchange related to the oxo component, both during crystallization and during deprotonation induced by thermal annealing (such as in a sample at the border between potassic-arfvedsonite and potassic-ferro-richterite; Oberti *et al.*, 2016*b*).

Acknowledgements

The authors thank Paul M. Ashley (adjunct associate professor at the University of New England at Armindale, Australia) and Renato and Adriana Pagano for kindly providing samples from the Hoskins mine. Part of this work was supported by a Canada Research Chair in Crystallography and Mineralogy, and Discovery Grants from the Natural Sciences and Engineering Research Council of Canada, and by Canada Foundation for Innovation Grants, to FCH. Careful revisions by Gunnar Raade, Herta Effenberger and a further anonymous reviewer are gratefully acknowledged.

References

Ashley, P.M. (1986) An unusual manganese silicate occurrence at the Hoskins mine, Grenfell district,

https://doi.org/10.1180/minmag.2016.080.124 Published online by Cambridge University Press

New South Wales. *Australian Journal of Earth Sciences*, **33**, 443–456.

Ashley, P.M. (1989) Geochemistry and mineralogy of tephroite-bearing rocks from the Hoskins manganese mine, New South Wales, Australia. *Neues Jahrbuch für Mineralogie Abhandlungen*, **161**, 85–111.

Brown, I.D. and Shannon, R.D. (1973) Empirical bond-strength-bond-lengths curves for oxides. *Acta Crystallographica*, **A29**, 266–282.

Bruker (2003) *SAINT Software Reference Manual. Version 6*. Bruker AXS Inc., Madison, Wisconsin, USA.

Busing, W.R., Martin, K.O and Levy, H.A. (1962) *ORFLS*. Report ORNL-Tm-305. Oak Ridge National. Laboratory, Oak Ridge, Tennessee.

Cannillo, E., Germani, G. and Mazzi, F. (1983) *New Crystallographic Software for Philips PW11000 Single Crystal Diffractometer*. CNR Centro di Studio per la Cristallografia, Internal Report 2.

Della Ventura, G., Robert, J.-L. and Hawthorne, F.C. (1996) Infrared spectroscopy of synthetic (Ni,Mg,Co)-potassium-richterite. *Geochimica et Cosmochimica Acta*, spec. vol. **5**, 55–63.

Della Ventura, G., Robert, J.-L., Raudsepp, M., Hawthorne, F.C. and Welch, M. (1997) Site occupancies in synthetic monoclinic amphiboles: Rietveld structure-refinement and infrared spectroscopy of (nickel, magnesium, cobalt)-richterite. *American Mineralogist*, **82**, 291–301.

Della Ventura, G., Robert, J.-L., Hawthorne, F.C., Raudsepp, M. and Welch, M.D. (1998) Contrasting $^{[6]}$Al ordering in synthetic Mg- and Co-pargasite. *The Canadian Mineralogist*, **36**, 1237–1244.

Della Ventura, G., Hawthorne, F.C., Robert, J.-L., Delbove, F., Welch, M.D. and Raudsepp, M. (1999) Short-range order of cations in synthetic amphiboles along the richterite – pargasite join. *European Journal of Mineralogy*, **11**, 79–94.

Della Ventura, G., Hawthorne, F.C., Robert, J.-L. and Iezzi, G. (2003) Synthesis and infrared spectroscopy of amphiboles along the tremolite – pargasite join. *European Journal of Mineralogy*, **15**, 341–347.

Della Ventura, G., Oberti, R., Hawthorne, F.C. and Bellatreccia, F. (2007) FTIR spectroscopy of Ti-rich pargasites from Lherz and the detection of O^{2-} at the anionic O3 site in amphiboles. *American Mineralogist*, **92**, 1645–1651.

Eggleton, R.A. and Ashley, P.M. (1989) Norrishite, a new manganese mica, $K(Mn_2^{3+}Li)Si_4O_{12}$, from the Hoskins mine, New South Wales, Australia. *American Mineralogist*, **74**, 1360–1367.

Gottschalk, M. and Andrut, M. (1998) Structural and chemical characterization of synthetic (Na,K)-richterite solid solutions by EMP, HRTEM, XRD and OH-valence vibrational spectroscopy. *Physics and Chemistry of Minerals*, **25**, 101–111.

Hawthorne, F.C. and Della Ventura, G. (2007) Short-range order in amphiboles. Pp. 173–222 in: *Amphiboles: Crystal Chemistry, Occurrence and Health Issues* (F.C. Hawthorne, R. Oberti, G. Della Ventura and A. Mottana, editors). Reviews in Mineralogy & Geochemistry, **67**. Mineralogical Society of America and the Geochemical Society, Chantilly, Virginia, USA.

Hawthorne, F.C., Oberti, R., Cannillo, E., Sardone, N., Zanetti, A., Grice, J.D. and Ashley, P.M. (1995) A new anhydrous amphibole from the Hoskins mine, Grenfell, New South Wales, Australia: description and crystal structure of ungarettiite, $NaNa_2(Mn_3^{3+}Mn_2^{2+})Si_8O_{22}O_2$. *American Mineralogist*, **80**, 165–172.

Hawthorne, F.C., Della Ventura, G. and Robert, J.-L. (1996*a*) Short-range order of (Na,K) and Al in tremolite: An infrared study. *American Mineralogist*, **81**, 782–784.

Hawthorne, F.C., Della Ventura, G. and Robert, J.-L. (1996*b*) Short-range order and long-range order in amphiboles: A model for the interpretation of infrared spectra in the principal OH-stretching region. *Geochimica et Cosmochimica Acta*, spec. vol. **5**, 49–54.

Hawthorne, F.C., Della Ventura, G., Robert, J.-L., Welch, M.D., Raudsepp, M. and Jenkins, D.M. (1997) A Rietveld and infrared study of synthetic amphiboles along the potassium-richterite – tremolite join. *American Mineralogist*, **82**, 708–716.

Hawthorne, F.C., Welch, M.D., Della Ventura, G., Shuangxi Liu, Robert, J.-L. and Jenkins, D.M. (2000) Short-range order in synthetic alluminous tremolites: an infrared and triple-quantum MAS NMR study. *American Mineralogist*, **85**, 1716–1724.

Hawthorne, F.C., Oberti, R., Harlow, G.E., Maresch, W.V., Martin, R.F., Schumacher, J.C. and Welch, M.D. (2012) Nomenclature of the amphibole supergroup. *American Mineralogist*, **97**, 2031–2048.

Kalinin, V.V., Marsiy, I.M., Dikov, Yu.P., Troneva, N.V. and Trubkin, N.V. (1992) Namansilite $NaMn^{3+}Si_2O_6$: A new silicate. *Proceedings of the Russian Mineralogical Society*, **I**, 89–94.

Kawachi, Y., Coombs, D.S., Leake, B.E. and Hinton, R.W. (2002) The anhydrous amphibole ungarettiite from the Woods mine, New South Wales, Australia. *European Journal of Mineralogy*, **14**, 375–377.

North, A.C.T., Phillips, D.C. and Mathews, F.S. (1968) A semi-empirical method of absorption correction. *Acta Crystallographica*, **A24**, 351–359.

Oberti, R., Cámara, F., Ottolini, L. and Caballero, J.M. (2003) Lithium in amphiboles: detection, quantification, and incorporation mechanisms in the compositional space bridging sodic and ^{B}Li-amphiboles. *European Journal of Mineralogy*, **15**, 309–319.

https://doi.org/10.1180/minmag.2016.080.124 Published online by Cambridge University Press

Oberti, R., Hawthorne, F.C., Cannillo, E. and Cámara, F. (2007) Long-range order in amphiboles. Pp. 125–172 in: *Amphiboles: Crystal Chemistry, Occurrence and Health Issues* (F.C. Hawthorne, R. Oberti, G. Della Ventura and A. Mottana, editors). Reviews in Mineralogy & Geochemistry, **67**. Mineralogical Society of America and the Geochemical Society, Chantilly, Virginia, USA.

Oberti, R., Boiocchi, M., Hawthorne, F.C., Ball, N.A. and Ashley, P.M. (2016*a*) Oxo-mangani-leakeite from the Hoskins mine, New South Wales, Australia: occurrence and mineral description. *Mineralogical Magazine*, **80**, 1013–1021, https://doi.org/10.1180/minmag.2016.080.037

Oberti, R., Boiocchi, M., Zema, M. and Della Ventura, G. (2016*b*) Synthetic potassic-ferro-richterite: 1. Composition, crystal structure refinement and HT behavior by *in operando* single-crystal X-ray diffraction. *The Canadian Mineralogist*, **54**, 353–369.

Reece, J.J., Redfern, S.A.T., Welch, M.D., Henderson, C. M.B. and McCammon, C.A. (2002) Temperature-dependent Fe^{2+}–Mn^{2+} order–disorder behaviour in amphiboles. *Physics and Chemistry of Minerals*, **29**, 562–570.

Robert, J.-L., Beny, J.-M., Beny, C. and Volfinger, M. (1989) Characterization of lepidolites by Raman and infrared spectrometries. I. Relationship between OH-stretching wavenumbers and composition. *The Canadian Mineralogist*, **27**, 225–235.

Robert, J.-L., Della Ventura, G. and Hawthorne, F.C. (1996) Infrared characterization of (OH-F)-pargasites. *Physics and Chemistry of Minerals*, **23**, 307.

Robert, J.-L., Della Ventura, G. and Hawthorne, F.C. (1999) Near-infrared study of short-range disorder of OH and F in monoclinic amphiboles. *American Mineralogist*, **84**, 86–91.

Robinson, K., Gibbs, G.V. and Ribbe, P.H. (1971) Quadratic elongation: a quantitative measure of distortion in coordination polyhedra. *Science*, **172**, 567–570.

Sheldrick, G.M. (1996). *SADABS Siemens Area Detector Absorption Correction Program*. University of Göttingen, Göttingen, Germany.

Tait, K.T., Hawthorne, F.C., Grice, J.D., Ottolini, L. and Nayak, V.K. (2005) Dellaventuraite, $NaNa_2(MgMn^{3+}_2Ti^{4+}Li)Si_8O_{22}O_2$, a new anhydrous amphibole from the Kajlidongri Manganese Mine, Jhabua District, Madhya Pradesh, India. *American Mineralogist*, **90**, 304–309.

Tyrna, P.L. and Guggenheim, S. (1991) The crystal structure of norrishite, $KLiMn^{3+}_2.Si_4O_{12}$: An oxygen-rich mica. *American Mineralogist*, **76**, 266–271.

https://doi.org/10.1180/minmag.2016.080.124 Published online by Cambridge University Press